TECHNICAL PROGRESS REPORT

For Period Ending 9-30-05
(April 1, 2005 to September 30, 2005)

Award Number DE-FC26-03NT41964

Sponsor: DOE Pittsburgh Energy Technology Center

Design, Synthesis, and Mechanistic Evaluation of Iron-Based Catalysis for Synthesis Gas Conversion to Fuels and Chemicals

Akio Ishikawa, Manuel Ojeda, and Enrique Iglesia
Department of Chemical Engineering
University of California at Berkeley
Berkeley, CA 94720

DISCLAIMER:

ABSTRACT

This project extends previously discovered Fe-based catalysts to hydrogen-poor synthesis gas streams derived from coal and biomass sources. These catalysts have shown unprecedented Fischer-Tropsch synthesis rate, selectivity for feedstocks consisting of synthesis gas derived from methane. During the first reporting period, we certified a microreactor, installed required analytical equipment, and reproduced synthetic protocols and catalytic results previously reported. During the second reporting period, we prepared several Fe-based compositions for Fischer-Tropsch synthesis and tested the effects of product recycle under both subcritical and supercritical conditions. During the third reporting period, we improved the catalysts preparation method, which led to Fe-based FT catalysts with the highest FTS reaction rates and selectivities so far reported, a finding that allowed their operation at lower temperatures and pressures with high selectivity to desired products (C_{5+}, olefins).

During this fourth reporting period, we have determined the effects of different promoters on catalytic performance. More specifically, we have found that the sequence in which promoters are introduced has a marked positive impact on rates and selectivities. Cu or Ru chemical promoters should be impregnated before K to achieve higher Fischer-Tropsch synthesis rates. The catalyst prepared in this way was evaluated for 240 h, showing a high catalytic activity and stability after an initial period of time necessary for the formation of the active phases. Concurrently, we are studying optimal activation procedures, which involve the reduction and carburization of oxide precursors during the early stages of contact with synthesis gas. Activation at low temperatures (523 K), made possible by optimal introduction of Cu or Ru, leads to lower catalyst surface area than higher activation temperatures, but to higher reaction rates, because such low temperatures avoid concurrent deactivation during the reduction-carburization processes. In this reporting period, we have measured the evolution of oxide, carbide, and metal phases of the active iron components using advanced synchrotron techniques based on X-ray absorption spectroscopy. These studies have revealed that Zn inhibits the isothermal reduction and carburization of iron oxide precursors. The concurrent presence of Cu or Ru compensates for these inhibitory effects and lead to the formation of active carbide phases at the low temperatures required to avoid deactivation via carbon deposition or sintering. Finally, we have also examined the kinetic behavior of these materials, specifically the effects of H_2, CO, and CO_2 on the rates and selectivities of Fischer-Tropsch synthesis reactions. This has led to a rigorous rate expressions that allows the incorporation of these novel materials into larger scale reactors and to predictions of performance based on the coupling of hydrodynamic and kinetic effects ubiquitous in such reactors.

TABLE OF CONTENTS

EXECUTIVE SUMMARY

This project exploits our recent discovery of catalyst compositions and synthesis and activation protocols leading to iron-based catalysts with Fischer-Tropsch synthesis (FTS) rates and sectivities similar to those on cobalt-based catalyst at low temperatures required to form olefins and large hydrocarbons using stoichiometric synthesis gas. These materials are being extended to the conversion of substoichiometric streams to explore whether the unprecedented activities and selectivities with streams derived from natural gas can be realized with more demanding coal-derived synthesis gas ratios. Fe catalysts convert streams derived from coal and biomass, because O-atoms are rejected as CO_2 instead of H_2O, but they tend to be much less active than Co catalysts, which reject O-atoms as H_2O. Fe catalysts are often less stable, because phase transformations can lead to structural disintegration. Higher FTS rates, lower CO_2 selectivities, and greater structural stability remain critical hurdles in converting H_2-poor streams to high-value fuels and chemicals. During the first reporting period, we certified a microreactor, installed required analytical tools, and reproduced previous synthetic protocols and catalytic results. During the second reporting period, we prepared several Fe-based compositions for Fischer-Tropsch synthesis and tested the effects of product recycle under both subcritical and supercritical conditions. During the third reporting period, we improved catalyst synthesis protocols, and achieved the highest FTS reaction rates and selectivities so far reported at the low temperatures required for selectivity and stability.

During this fourth reporting period, we have studied the effects of different promoters on catalytic performance. We have found that the sequence used to introduce promoters strongly influences rates and selectivities. Cu or Ru chemical promoters impregnated before K lead to higher Fischer-Tropsch synthesis rates and catalysts thus prepared showed high rates, selectivities, and stability during extended tests of 240 h after an initial period of time required to form active phases. We have also examined optimal activation procedures, involving reduction and carburization of oxide precursors during early stages of contact with synthesis gas. Activation at low temperatures (523 K), made possible by optimal Cu or Ru promotion led to lower catalyst surface areas than higher activation temperatures, but to higher reaction rates, because low temperatures avoid concurrent deactivation during reduction-carburization. We have measured the evolution of oxide, carbide, and metal phases of active Fe components using synchrotron-based X-ray absorption spectroscopy. These studies have revealed that Zn inhibits the isothermal reduction and carburization of iron oxide precursors. The concurrent presence of Cu or Ru compensates for these inhibitory effects and lead to the formation of active carbide phases at the low temperatures required to avoid deactivation via carbon deposition or sintering. Finally, we have also examined the kinetic behavior of these materials, specifically the effects of H_2, CO, and CO_2 on the rates and selectivities of Fischer-Tropsch synthesis reactions. This has led to a rigorous rate expressions that allows the incorporation of these novel materials into larger scale reactors and to predictions of performance based on the coupling of hydrodynamic and kinetic effects ubiquitous in such reactors.

Design, Synthesis, and Mechanistic Evaluation of Iron-Based Catalysis for Synthesis Gas Conversion to Fuels and Chemicals

Description of Tasks

Task One (Years 1 and 2)
Extension of synthesis and activating protocols for Fe-based catalysts prepared by precipitation, treatment with surface-active agents, activation in synthesis gas, and promotion by Ru to materials suitable Fischer-Tropsch synthesis with coal- and biomass-derived synthesis gas.

Task Two (Years 1 and 2)
Characterization of carbide-oxide phase transformations and their impact on catalyst mechanical integrity using electron microscopy and in situ X-ray absorption protocols.

Task Three (Years 2 and 3)
Exploratory studies of the effects of CO_2 and light hydrocarbon recycle on the rate and selectivity of FTS reactions at low H_2/CO ratios on optimized Fe-based catalysts (developed in part (i)).

Objectives and Specific Tasks

Fe-based catalysts are typically preferred for converting coal or biomass derived synthesis gas streams with low H_2/CO ratios (H_2/CO = 0.7-1) because their significant water-gas shift activity ($H_2O + CO \rightarrow CO_2 + H_2$) leads to rejection of excess carbon as CO_2. Fe-based catalysts typically show much lower catalytic activities than Co-based catalysts and lower mechanical stability, as a result of their tendency to interconvert between oxide and carbide phases as the redox properties change within catalytic reactors. Fe-based catalysts with higher Fischer-Tropsch Synthesis (FTS) activity and greater structural integrity remain significant obstacles to their use in the synthesis of high-value fuels and petrochemicals.

Iron-based catalysts with FTS activities and selectivities similar to those on cobalt-based catalyst using stoichiometric H_2/CO streams derived from natural gas were recently reported by our research group. Novel synthesis methods based on supercritical and subcritical drying of powders after precipitation at a constant pH led to significant improvements in the surface area of oxide precursors, while activation and promotion protocols led to active Fe carbide clusters with high surface areas and mechanical strength. These gave in turn unprecedented activity and C_5^+ selectivity during use with stoichiometric synthesis gas (H_2/CO = 2).

The principal objectives of this project are to:

1. optimize synthesis protocols to prepare Fe-based catalysts with FTS rates and hydrocarbon product distributions similar to those of Co-based materials using surface-active compounds and supercritical conditions and explore the use of Ru as activation promoter,

2. evaluate the performance of prepared catalysts in synthesis gas streams derived from coal or biomass (H_2/CO = 0.7-1.0) and optimize activation protocols for high activity, selectivity and mechanical integrity,

3. determine the effects of Ru loading and mode of addition on the concentration of active sites and on the intrinsic activity and selectivity of such active sites,

4. establish the extent and dynamics of carbide-oxide transformations during reactions of synthesis gas mixtures with varying redox potential and their influence on the structural integrity and stability of Fe-based catalysts.

Technical Activities and Accomplishments (FY 2005)

During this fourth reporting period, we have prepared and characterized some Fe-based catalysts and we have measured their Fischer-Tropsch synthesis reaction rates and selectivities. These studies have

(1) established an appropriate method of iron-based catalysts promotion, resulting in the improvement of the catalytic activity compared to the previous work,
(2) tested and confirmed the high catalytic stability of the samples prepared according to our findings,
(3) shown that the activation of iron-based catalysts at low temperature (523 K) in synthesis gas leads to a more active catalysts than those activated at 543 or 573 K,
(4) demonstrated the promoting effects of Cu (or Ru) and K in enhancing the reduction and carburization of iron oxide precursors and the inhibitory effects of ZnO components used as structural promoters to preserve high surface areas,
(5) determined the kinetic influence of the hydrogen and carbon monoxide partial pressure on catalytic rates and selectivities.

The detailed results, findings, and conclusions are included in the last part of this report as sections:

2.1. Prepared Catalysts and BET Surface Area.

2.2. Fischer-Tropsch Synthesis on Iron-based Catalysts with Hydrogen-poor synthesis gas.

2.2.1. Effect of promoter order addition on Fisher-Tropsch Synthesis rates and selectivities.

2.2.2. Catalytic performance of Fe-Zn-Cu_3-K_6 in Fischer-Tropsch Synthesis.

2.3. Structure Evolution and Site Requirements in Fe-Catalyzed Fischer-Tropsch Synthesis.

2.3.1. Catalytic behavior of Fe-based catalysts during isothermal activation.

2.3.2. Structure evolution during the activation process.

2.4. Kinetic Study of the Fischer-Tropsch Synthesis with Iron-based Catalyst.

2.4.1. Influence of H_2 partial pressure on reaction rates and product selectivity.

2.4.2. Influence of CO partial pressure on reaction rates and product selectivity.

2.4.3. Mechanism and kinetics of hydrocarbons formation.

Immediate Next Steps and Research Plans are:

During the next reporting period, we will continue to investigate the optimum activating protocols for Fe-based catalysts in order to obtain catalysts with high activity, selectivity and mechanical integrity. More specifically, we intend to determine the optimum time and temperature values required in order to maximize the rate of hydrocarbons formation. We will also correlate the transient and final catalytic performance with the different structures present in the catalyst, which will lead to a better comprehension of the active phase for the Fischer-Tropsch Synthesis. In addition, we will complete kinetic study that we have started during this reporting period. We will address the detailed kinetic response of optimized catalysts to different reactants partial pressure (H_2, CO, CO_2,…). We will optimize and improve the reaction mechanisms reported in this period, and we will derive more rigorous kinetic rate expressions required for scale up in more complex hydrodynamic systems of industrial importance. Finally, the comparison between the experimental data and those predicted with the different models will shed light on the reaction mechanism for hydrocarbons formation. During this penultimate reporting period, we will start the assembly of a final report containing all findings of this project.

Detailed results, findings and conclusions

1. Experimental details

1.1. Synthesis of Precursors and Catalysts

The addition of promoters to Fe-Zn oxide precursors was accomplished following two different procedures, which are shown in Scheme 1. The aqueous solutions of K_2CO_3, $Cu(NO_3)_2$, or ruthenium (III) nitrosylnitrate $[Ru(NO)(NO_3)_x(OH)_y$ $(x+y = 3)]$ were used as the sources of K, Cu and Ru. The first process (Route 1) was carried out according to the previously reported work. First, potassium was added by incipient wetness impregnation with solutions with the required concentration to obtain the desired K/Fe atomic ratio (K/Fe = 0.06). Next the solid was dried overnight at 393 K in ambient air. Cu or Ru were then added at a Cu/Fe and Ru/Fe atomic ratio of 0.03 (Cu(Ru)/Fe = 0.03) in a second step, followed by overnight drying at 393 K in ambient air. Finally, the samples were treated in flowing dry air at 543 K for 4 h. The resulting oxide precursors are denoted throughout as Fe-Zn-K_6, Fe-Zn-K_6-Cu_3, and Fe-Zn-K_6-Ru_3, respectively. The other process (Route 2) was carried out as follows. First, Cu or Ru were added to the Fe-Zn oxide precursor at Cu(Ru)/Fe atomic ratios (Cu(Ru)/Fe = 0.03), followed by overnight drying at 393 K in ambient air and drying at 543 K for 4 h in flowing dry air. Potassium was then added at K/Fe atomic ratios (K/Fe = 0.06) in the second step, followed by overnight drying at 393 K in ambient air. These samples were again treated in flowing dry air at 543 K for 4 h. The resulting oxide precursors are denoted as Fe-Zn-Cu_3-K_6 and Fe-Zn-Ru_3-K_6, respectively.

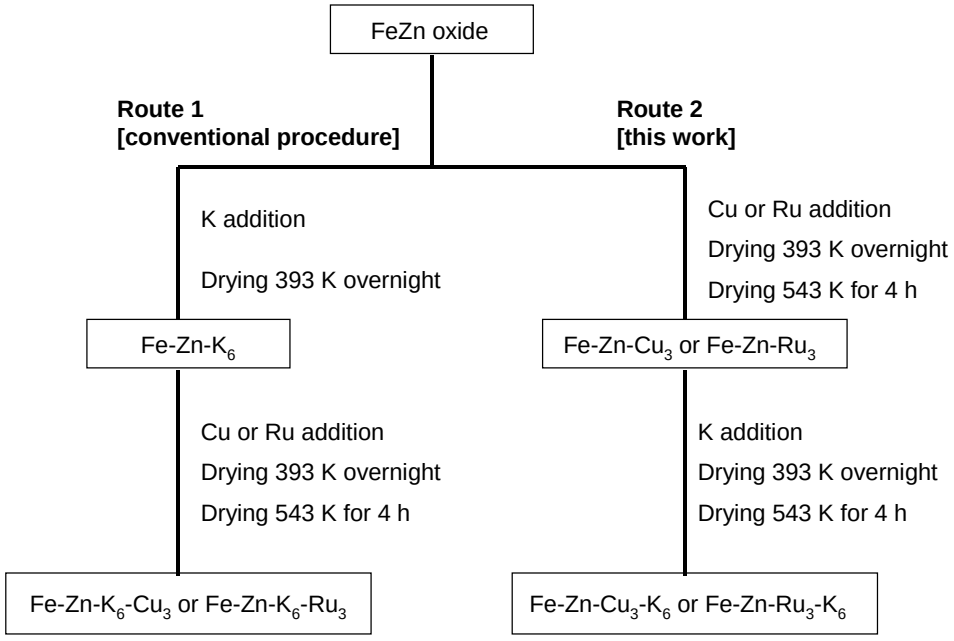

Scheme 1. Procedure for preparation of iron-based catalysts with promoters.

1.2. Fischer-Tropsch Synthesis Reaction and Product Selectivity

Fischer-Tropsch synthesis rates and selectivites were measured in a single-pass packed-bed reactor with plug-flow hydrodynamics. This reactor was held within a resistively-heated three-zone furnace. All lines after the reactor were kept at 433-553 K and a vessel placed immediately after the reactor was held at 408 K to collect liquid products. Reactant and product streams were analyzed online using a gas chromatograph (Agilent Technologies, model 6890N). The analysis of N_2, CO, CO_2, and CH_4 was performed using a thermal conductivity detector and a Porapak Q packed-column (15.2 cm × 0.318 cm diameter). All hydrocarbons up to C_{15} were analyzed on-line using flame ionization detection and a cross-linked methyl silicone capillary column (HP-1, 50 m×0.32 mm; 1.05 μm film).

Fe catalysts (100-180 μ, 0.4 g) were diluted with 11 g of quartz granules (100-180 μ) to avoid temperature gradients. Quartz granules were washed with concentrated nitric acid and treated in air at 973 K before use. Catalysts were activated using flowing synthesis gas (H_2/CO = 2) at 0.1 MPa by increasing the temperature from 298 to 423 K at a rate of 10 K/min and from 423 to 543 K at 1 K/min. The catalysts were held at 543 K for 1 h. After activation, the temperature was decreased to 508 K, and the synthesis gas (H_2/CO = 1) pressure was gradually increased to 2.14 MPa. FTS reactions were carried out with the synthesis gas (Praxair; H_2/CO/N_2 mixture; (i) 0.62/0.31/0.07 [H_2/CO = 2], or (ii) 0.46/0.46/0.08 mol [H_2/CO = 1]) as reactant at 2.14 MPa gas pressure and 508 K.

2. Results and Discussion

2.1. Prepared Catalysts and BET Surface Area

The list of prepared catalysts and BET surface areas are summarized in Table 2.1. The surface area measured by N_2 adsorption at 77 K were 251-291 m^2/g for oxyhydroxide precipitates obtained by drying in ambient air at 393 K. The surface area for Fe-Zn oxides decreased after drying in flowing air at 543 K for 4 h. The addition of K, Cu and/or Ru promoters to Fe-Zn oxides also decreased their surface area, apparently because of pore collapse.

Table 2.1. List of prepared catalysts and BET surface area.

Catalyst	Relative composition (at.)					BET surface area
	Fe	Zn	K	Cu	Ru	m^2/g-cat
FeZn	100	10	-	-	-	198
$FeZnK_6Cu_3$	100	10	6	3	-	141
$FeZnK_6Ru_3$	100	10	6	-	3	147
$FeZnCu_3K_6$	100	10	6	3	-	159
$FeZnRu_3K_6$	100	10	6	-	3	183

2.2. Fischer-Tropsch Synthesis on iron-based catalysts with hydrogen-poor synthesis gas stream.

2.2.1. Effect of promoter order addition on Fischer-Tropsch Synthesis rates and selectivities.

The FTS rates and selectivities on the prepared catalysts are shown in Table 2.2. CO conversion rates increased with Ru or Cu addition to Fe-Zn-K, suggesting that Ru and Cu species promote catalyst carburization and reduction rates. This promoter effect can be attributed to a larger number of active sites or to the formation of active sites with a higher intrinsic activity. The rate of CO conversion and hydrocarbon formation was higher on Fe-Zn-Cu_3-K_6 and Fe-Zn-Ru_3-K_6 than on Fe-Zn-K_6-Cu_3 and Fe-Zn-K_6-Ru_3. Those different activities were caused by the two different protocols of promoter addition. Aqueous solutions of $Cu(NO_3)_2$ and $Ru(NO)(NO_3)_x(OH)_y$ were used as sources of Cu and Ru. The pH values for aqueous Cu and Ru complexes solutions were ca. 3 and 0.3, respectively. In the case of Fe-Zn-Cu_3-K_6 and Fe-Zn-Ru_3-K_6, which display high catalytic activities, Cu or Ru were first deposited on the Fe-Zn oxide precursors, dried at 543 K for 4 h in flowing dry air and then K was added. For Fe-Zn-K_6-Cu_3 and Fe-Zn-K_6-Ru_3 samples were obtained by adding of K first and then Cu or Ru. Finally, the catalytic precursors were dried at 543 K for 4 h in flowing dry air. Therefore, this procedure implies that acidic solutions of Cu and Ru solution were added to Fe-Zn oxide and K_2CO_3 particles on the surface of the precursor. It seems that the neutralization reaction of acidic species and K_2CO_3 accompanies this addition of metal nitrate solutions, suggesting that those reactions led to the condensation of Cu or Ru hydroxides and to the decomposition of K_2CO_3. In the case of Fe-Zn-K_6-Cu_3 and Fe-Zn-K_6-Ru_3 samples, it appeared that the condensation of Cu or Ru hydroxides and the decomposition of K_2CO_3 led to higher CH_4, lower C_5^+ selectivity and to lower FTS rates.

The procedure that we propose here for the addition of the catalytic promoters can result in Fe-Zn-Cu_3-K_6 and Fe-Zn-Ru_3-K_6 catalysts with a superior FTS catalytic rates compared to Fe-Zn-K_6-Cu_3 and Fe-Zn-K_6-Ru_3 catalysts prepared by the conventional procedure. Besides, we have found that the Fe-Zn-Cu_3-K_6 catalyst showed the highest FTS performance among all the catalysts here studied.

Table 2.2. Steady-state performance of Fe_2O_3-Zn catalysts (Zn/Fe=0.1) with different loadings of K, Cu, and Ru. (H_2/CO=1, 508 K, 2.14 MPa, CO conversion 12-18%).

	Fe-Zn-K_6	Fe-Zn-K_6-Cu_3	Fe-Zn-Cu_3-K_6	Fe-Zn-K_6-Ru_3	Fe-Zn-Ru_3-K_6
CO conversion rate (mol CO/h.g-at. Fe)	2.2	4.4	6.7	3.2	5.1
Hydrocarbon formation rate (mol CO/h.g-at. Fe)	1.6	3.2	5.1	2.2	3.6
CO_2 selectivity (%)	17.3	28.3	25.9	31.5	30.7
CH_4 selectivity (%) [a]	3.9	2.8	1.9	4.5	2.7
C_5^+ selectivity (%) [a]	84.0	85.7	87.6	80.0	85.5
1-C_5H_{10}/*n*-C_5H_{12} ratio	2.5	2.8	3.1	2.5	2.7

[a] CH_4 and C_5^+ selectivities are reported on a CO_2-free basis.

2.2.2. Catalytic performance of Fe-Zn-Cu_3-K_6 in Fischer-Tropsch Synthesis.

The Fischer-Tropsch synthesis was carried on Fe-Zn-Cu_3-K_6 out at 508 K and 2.14 MPa under synthesis gas stream (5.0 NL/h/g-cat.) with H_2/CO = 1 for 240 h to examine the stability of this catalytic material. Figure 2.1 shows the dependence of the hydrocarbon formation rate with the time-on-stream (TOS) under synthesis gas (H_2/CO = 1). The rate of hydrocarbon formation over Fe-Zn-Cu_3-K_6 decreases rapidly during the initial stages of reaction (ca. 9 h). In this initial period, the sharp decrease in hydrocarbon synthesis rates appears to reflect a decrease of the surface area as a consequence of the carbide-oxide transformations, which take place when synthesis gas contacts the Fe oxide precursors at our reaction conditions (508 K and 2.14 MPa). After this initial period, the hydrocarbon formation rate on Fe-Zn-Cu_3-K_6 decreases gradually and slowly. The following two possibilities can explain this second decrease of the hydrocarbon formation rate. In one case, the catalyst can continuously deactivate as a consequence of the formation of inactive species, such as carbonaceous deposits, on the catalyst surface. In the other case, it is also possible that a small amounts of catalyst granules (or even catalytic promoters) are removed out of the reactor by liquid products that leave as such in the trickle-bed operation of these packed-bed reactors. Although the catalyst deactivation by unreactive residues cannot be ruled out, it seems that the decrease of the hydrocarbon formation rate is better explained by the removal of the catalyst (or catalytic promoters) from the catalytic bed. This is supported by the fact that the waxes collected after the reactor display a black color, suggesting that Fe carbides are probably contained within such liquid hydrocarbon streams.

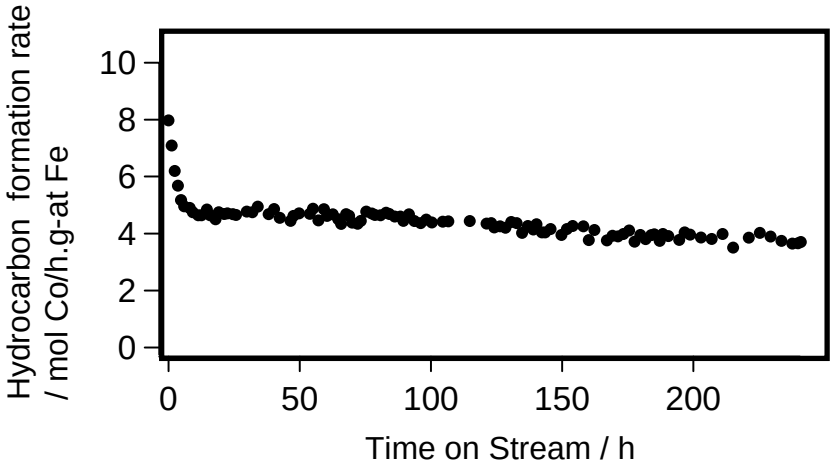

Figure 2.1. Hydrocarbon formation rates with time on stream (H_2/CO=1, SV=5.0 NL/h.g-cat) at 508 K and 2.14 MPa.

The improvement of the experimental method may result in more steady FTS rates on Fe-Zn-Cu_3-K_6. Here, we compare FTS reaction rates and selectivities on a Fe-Zn-Cu_3-K_6 catalyst with those on previously reported Fe-based catalysts. Fe-Zn-Cu_3-K_6 samples are compared with the most active reported Fe-based catalysts in Table 2.3 at relatively high CO conversions. CO conversion rates and hydrocarbon synthesis productivities on Fe-Zn-Cu_3-K_6 with a synthesis gas stream containing H_2/CO = 1.0 at 508 K are higher than those reported on Fe-SiO_2-$K_{5.9}$-$Cu_{4.4}$ (H_2/CO = 2.0). The additional investigations of synthesis, promotion and activation protocols in order to increase the density of FTS active site have led to additional improvements in hydrocarbon synthesis productivities.

Table 2.3. Steady State FTS Performance of Various Fe-Based Catalysts Using Natural Gas-Derived Synthesis Gas (H_2/CO = 1.0-2.0).

	Fe-Zn-Cu_3-K_6	Fe-Zn-K_6-Cu_3	Fe-Zn-K_4-Cu_2	Fe-SiO_2-$K_{5.9}$-$Cu_{4.4}$
	This work	Previous work	Ref 1	Ref 2
Reactor Type	Fixed-bed	Fixed-bed	Fixed-bed	Spinning Basket
Temperature (K)	508	508	508	523
Pressure (MPa)	2.14	2.14	2.14	2.4
H_2/CO ratio	1.0	1.0	2.0	2.0
CO conversion (%)	52.2	47.0	50.8	52.7
Hydrocarbon productivity (g/h.kg-cat)	645	415	765	404

Ref 1: S. Li *et al.*, J. Catal. 206 (2002) 202.

Ref 2: van der Laan *et al.*, Ind. Eng. Chem. Res. 38 (1999) 1277.

2.3. Structural Evolution and Site Requirements in Iron-Catalyzed Fischer-Tropsch Synthesis.

2.3.1. Catalytic behavior of Fe-based catalysts during isothermal activation process.

During the third reporting period, we reported the FTS performance on several iron-based catalysts under synthesis gas stream at 508 K and 2.14 MPa. Those catalysts were activated at 543 K for 1 h under synthesis gas stream before the FTS reaction was carried out. However, the optimum activation procedure has not been investigated for those catalysts. It is expected that further optimization would lead to even higher FTS rates. We examine here this premise.

During this reporting period, we have measured the FTS performance on Fe_2O_3, Fe-Zn oxide, and Fe-Zn-Cu_3-K_6 catalysts previously activated under an isothermal activation process (523 K) in order to evaluate the relationship between catalyst activation time and FTS performance. These isothermal activation processes were carried out after treating the samples in He (100 cm^3 min^{-1}) at 573 K for 1 h. Figure 2.2 shows the product formation rates over Fe_2O_3, Fe-Zn oxide, and Fe-Zn-Cu_3-K_6 during the activation process with synthesis gas H_2/CO=2 at 523 K. It can be observed that methane and hydrocarbons are immediately formed on Fe_2O_3, Fe-Zn-Cu_3-K_6 after contact with synthesis gas, and then rates increased with time on stream. This indicates that the active sites on catalysts for FTS reaction were immediately formed after the synthesis gas contact. On the other hand, hydrocarbons are formed over Fe-Zn oxide after an induction period (ca 5 h). Several iron phases, such as Fe_3O_4 and Fe_3C, have been postulated in the literature to be the active sites for hydrocarbon formation. It seems that the formation of the Fe_3O_4 and Fe carbide phases on Fe-Zn oxide without promoters took place slowly during the induction period, probably because of the Zn effect, that is, Zn seems to inhibit the reduction and carburization of the iron phase. The hydrocarbon and CH_4 formation rates on Fe-Zn oxide increased after ~ 5 h.

After 25 h time-on-stream, the CH_4 formation rate on Fe-Zn oxide was ~ 0.03 mmol/s/g-atom Fe, more than 3 times larger than the methane formation rate on Fe-Zn-Cu_3-K_6. On the other hand, Fe-Zn-Cu_3-K_6 showed the highest C_5^+ selectivity (data not shown). These different FTS selectivities were caused by the presence of potassium promoter.

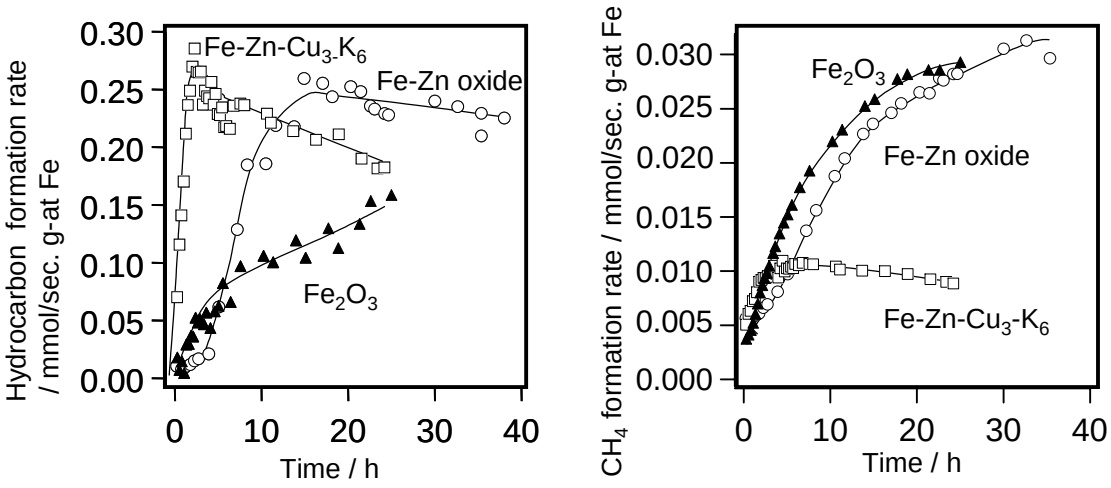

Figure 2.2. CH_4 and hydrocarbon (C_1-C_9) formation rates on iron-based catalysts during activation process. (0.2 g sample; H_2/CO = 2, flow rate: 108 mol/h. g-atom Fe, at 523 K and 0.1 MPa).

Therefore it was found that iron catalysts without promoters need to be activated for more that 20 h. The increase of FTS rates with the reaction time was observed on Fe-Zn-Cu_3-K_6 for ca 5 h after contact with synthesis gas, and then FTS rates decreased with time. It is expected that a further improvement of the activation time brings about the catalyst with higher activity.

2.3.2. Structure evolution during the catalyst activation process.

The structure and nature of the iron oxide phases and the reaction products formed during the catalyst activation process were measured by X-ray absorption spectroscopy and mass spectrometry to explore in detail the behavior of the catalysts during the activation step. The FTS rates on Fe_2O_3, Fe-Zn oxide, and Fe-Zn-Cu_3-K_6, shown in Figure **2.2,** indicate that the catalytic activities on the different catalysts cannot be evaluated on the basis of CH_4 formation rates alone because of the different FTS selectivities among these samples. However, the behavior of CH_4 formation rate for a fixed catalyst can be related to its rate of hydrocarbon formation. Therefore, it seems that the catalytic activity on the same catalyst can be evaluated by its rate of CH_4 formation. In this report, we explored the optimum activation procedure on the basis of the CH_4 formation rate accurately measured by mass spectrometry.

Figure 2.3 shows the rate of formation of CH_4, H_2O, and CO_2 on Fe-Zn-Cu_3-K_6 catalyst with synthesis gas (H_2/CO = 1, 108 mol/h. g-atom Fe) at 543 K and 0.1 MPa as a function of time on time on stream. Figure 2.3 shows also the concentrations of the Fe_2O_3, Fe_3O_4, and FeC_x phases obtained by near-edge X-ray absorption spectroscopy at the same reaction conditions (H_2/CO = 1, 543 K, 0.1 MPa) during transient FTS experiments. The X-ray absorption spectra of Fe-Zn-Cu_3-K_6 at 543 K changed with time on stream under synthesis gas. The spectra can be described as linear combinations of the near-edge spectra of the

three standard compounds (Fe_2O_3, Fe_3O_4, and FeC_x) identified by principal component analysis.

The lattice oxygen atoms are removed from Fe_2O_3 and CuO by H_2 to form H_2O or by CO to form CO_2 during contact with synthesis gas. Carbon is also deposited via CO disproportionation reactions that also form CO_2. Sharp peaks in CH_4, H_2O and CO_2 formation rates were observed after about 1 min of catalyst exposure to synthesis gas at 543 K. The removal of the lattice oxygen from CuO to form Cu metal occurs during this period because the CuO deposited on the catalyst surface is reduced easily to Cu metal at 543 K. However, the amount of removal oxygen during this initial period was larger than that of the lattice oxygen of CuO. X-ray absorption spectra showed that hematite (Fe_2O_3) disappears very quickly during this initial contact with synthesis gas, while Fe_3O_4 and FeC_x species were detected concurrently. The extent of catalyst carburization increased with the reaction time, while the fraction of magnetite (Fe_3O_4) decreased. After 45 min time on stream, the only iron phase detected was iron carbide (FeC_x). Therefore, the initial exposure of the catalyst to synthesis gas at 543 K also led to the removal of oxygen from the surface and bulk of Fe_2O_3 to form Fe_3O_4 and finally, to the introduction of carbon into the iron structure to form FeC_x. This latter process is very fast, as indicated by the observation that the concentration of FeC_x reached 20% after 1 min.

The carburization of an Fe oxide is an exothermic reaction. This is supported by the increase of the reaction temperature that we observed after the initial contact between the synthesis gas and the catalyst. The increase of the catalyst temperature as a result of the sudden formation of the FeC_x species at the beginning of the reaction (1 min) seems to be the reason of the sharp peaks corresponding to the formation of CH_4, H_2O and CO_2 in Figure 2.3.

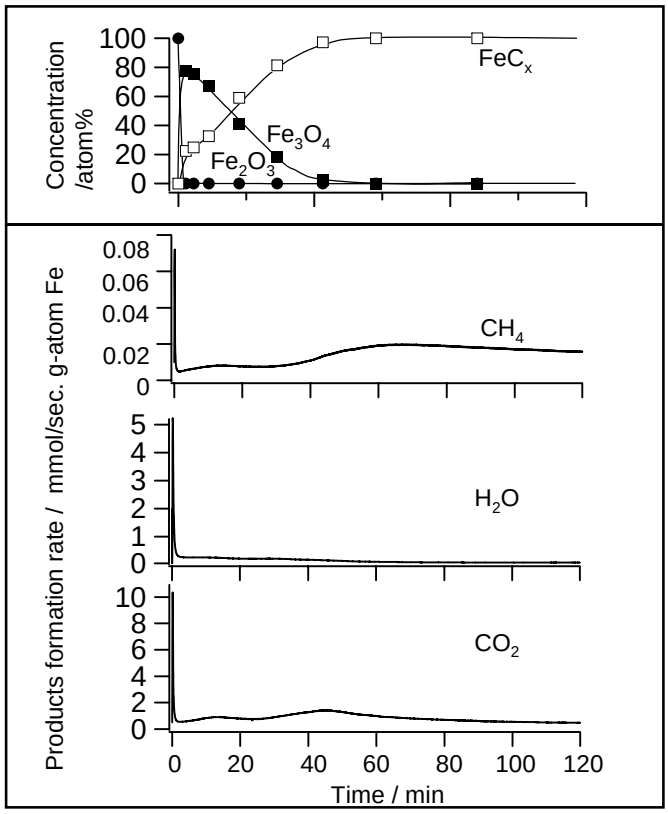

Figure 2.3. Structural evolution obtained from XAS (1 mg sample, 543 K) and rate of formation of CH_4, H_2O, and CO_2 as a function of time on Fe-Zn-Cu_3-K_6 (0.2 g sample, 543 K). Synthesis gas: H_2/CO = 1, Flow rate: 108 mol/h. g-atom Fe.

As described before, a sharp peak corresponding to the rate of water formation is observed initially. Following, the water formation rate decreased with time on stream. The behavior of CH_4 and CO_2 is different. In this case, two broad formation rate peaks were observed. The first CO_2 formation rate peak is attributed to the reduction of hematite to form magnetite, while the second peak is consequence of the iron carbides formation. It also seems that the first broad peak of the CH_4 formation rate is mainly attributed to the CH_4 formation on Fe_3O_4 species, which means that Fe_3O_4 is also an active species for Fischer-Tropsch reaction. The other methane formation rate peak is attributed to the CH_4 formation on FeC_x species. The rate of CH_4 formation reached the maximum value when the FeC_x concentration reached 100%, and then decreased slowly with time.

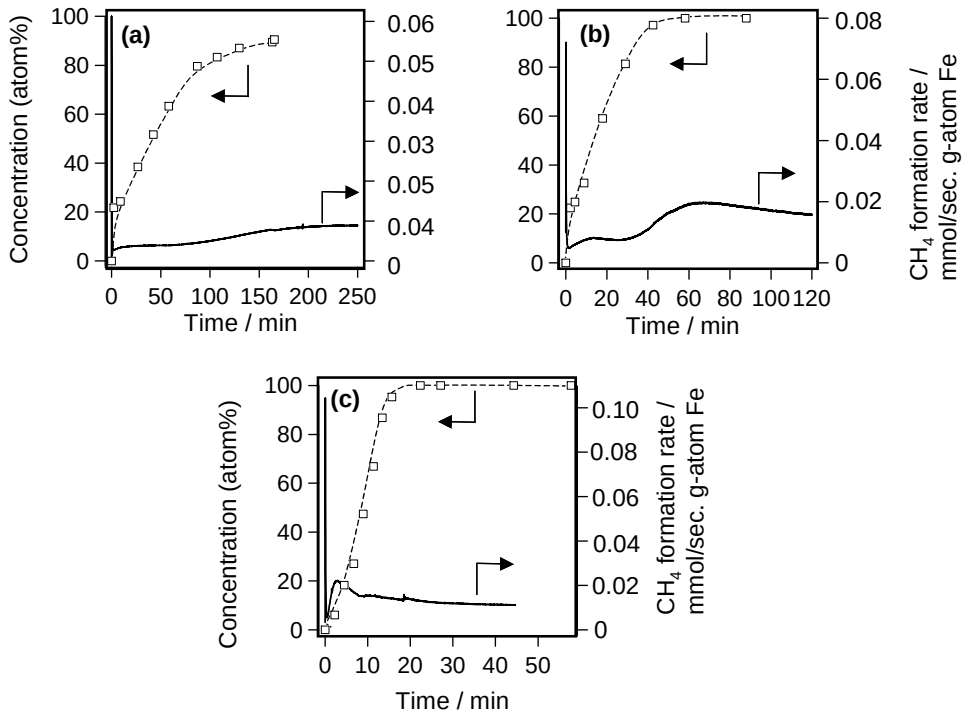

Figure 2.4. Fe carbide concentration (open mark) obtained from XAS (1 mg sample) and rate of formation of CH_4 as a function of time on Fe-Zn-Cu_3-K_6 (0.2 g sample) at (a) 523, (b) 543 and (c) 573 K. Synthesis gas: H_2/CO = 1, Flow rate: 108 mol/h. g-atom Fe.

Figure 2.4 shows the iron carbide concentrations obtained from *in situ* XAS on Fe-Zn-Cu_3-K_6 as a function of time at different reaction temperature. It can be observed that at 543 and 573 K, FeC_x contributions approached constant values of ca. 100% after 60 and 20 min respectively. On the other hand, the Fe_3O_4 and FeC_x contributions at 523 K were approximately 10% and 90%, respectively, after 180 min. Figure 2.4 also shows the CH_4 formation rates measured at the same reaction conditions as those used for the XAS experiments. The rate of CH_4 formation at 523 K increased with increasing FeC_x content. At 543 and 573 K, the rate of CH_4 formation increased with increasing FeC_x content and then decreased with the time on stream. At 573 K, the deactivation of catalyst took place after 5 min in contact with the synthesis gas. It seems that the decrease of CH_4 formation rates was caused by the formation of the inactive species, such as carbon, upon exposing the iron oxide to synthesis gas at high temperature. It was found that the deactivation of catalyst accompanied the activation process at high temperature.

FTS rates increase with increasing reaction temperature. To evaluate the optimum activation process by the CH_4 formation rate, it is necessary to measure this rate of CH_4 formation at the same conditions after the activation process. Table 2.4 summarizes the surface area of Fe-Zn-Cu_3-K_6 activated at various temperatures as well as the CH_4 formation rates measured at 508 K after different activation processes. The activation

processes at 543 and 573 K were carried out for 70 and 5 min, respectively, because according to the Figure 2.4, the Fe-Zn-Cu_3-K_6 catalyst needs to be activated for these periods of time in order to achieve the highest rate of CH_4 formation. The surface area of Fe-Zn-Cu_3-K_6 activated at 523 K for 300 min was the lowest value among all the samples and the FeC_x concentration was 90%. It seems that the activation at high temperature leads to the preferential nucleation of a new phase at multiple locations on the surface of an Fe_2O_3 crystallite because of the rapid reduction and carburization of the catalysts. Therefore, it appears that the increase of activation temperature results in the increase of the surface area. However, the Fe-Zn-Cu_3-K_6 activated at 523 K for 300 min showed the highest CH_4 formation rate, despite the fact that this sample displayed the lowest surface area. There are apparently two possibilities in order to explain this behavior. One of them is the rapid deactivation of catalyst activated at high temperature. The contact Fe-Zn-Cu_3-K_6 with synthesis gas at 573 K brought about the deactivation of catalyst just after 5 min in spite of the low FeC_x concentration (20%). The other possibility is that active sites formed via promoters have the satisfactory promoter effects. Cu and K species on the Fe_2O_3 surface promote the reduction and carburization of Fe_2O_3. The reduction and carburization of the Fe-Zn-Cu_3-K_6 catalyst at low temperature takes place because of the presence of the different promoters, while the reduction and carburization at high temperature, particularly at 573 K, takes place more easily, even without the presence of promoters. Therefore, at the higher temperatures, the reduction and carburization by H_2 and CO caused the lack of promoter effect on the formation of the active species during the reduction and carburization processes. According to our results, it appears that the Fe-Zn-Cu_3-K_6 catalyst activated at low temperature (523 K) with satisfactory promoter effects showed the highest CH_4 formation rate.

Table 2.4. Characterization results and CH_4 formation rate over Fe-Zn-Cu_3-K_6 activated a different temperature and time.

Temperature (K)	523	543	573
Activation time (min)	300	70 (120)	5 (45)
surface area after reaction (m^2/g)	14.6	26.9 (16.8)	42.5 (31.3)
Steady-state FeC_x [a] concentration (%)	90	100 (100)	20 (100)
Steady-state CH_4 formation [b] rate (mmol/sec. g-atom Fe)	0.0054	0.0052 (0.0047)	0.0039 (0.0031)

[a] FeC_x concentration measured after exposure to synthesis gas (1 mg Fe-Zn-Cu_3-K_6, H2/CO = 1, synthesis gas flow rate = 108 mol/h. g-atom Fe)

[b] CH_4 formation rates measured at 508 K after activation at various temperatures (0.2 g Fe-Zn-Cu_3-K_6, H_2/CO = 1, synthesis gas flow rate = 108 mol/h. g-atom Fe)

Up to this point, the activation procedure has been carried out systematically at 543 K for 1 h. However, these activation conditions has not been optimized in spite of the importance of this process for optimum FTS reaction. Our results suggest that catalyst activation at low temperature has a positive effect on its catalytic performance. The evaluation and optimization of FTS performance with different catalysts activated under the proposed activation procedure is currently under investigation and will be addressed during the next next reporting period.

2.4. Kinetic Study of the Fischer-Tropsch Synthesis on Iron-Based Catalyst.

The kinetics of the Fischer-Tropsch Synthesis (FTS) have been studied during this reporting period. The kinetic measurements have been performed on Fe-Zn-Cu_3-K_6, which was found to be the most active catalyst in previous studies. The ultimate objective of these experiments is to propose a reaction mechanism that describes and predicts the rates of formation of the various hydrocarbons formed during reactions of CO and H_2 on Fe-based catalysts and which can be used to embed into hydrodynamic models of complex practical reactors.

2.4.1. Influence of H_2 partial pressure on reaction rates and product selectivity.

We have measured the catalytic performance of Fe-Zn-Cu_3-K_6 at 508 K and constant CO partial pressure (P_{CO} = 0.40 MPa) but different H_2 partial pressures (P_{H2}= 0.40, 0.60, 0.80 and 1.00 MPa). Figure 2.5 shows the influence of H_2 partial pressure on the CO conversion at different values of CO space velocity. CO conversion rates increased with increasing hydrogen partial pressure.

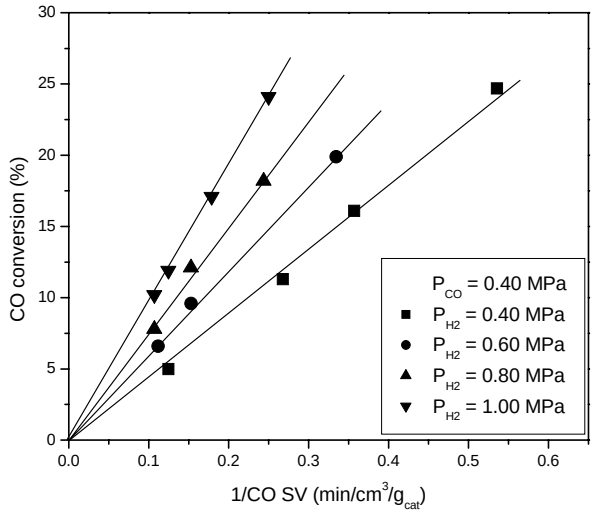

Figure 2.5. Influence of H_2 partial pressure on the CO conversion over Fe-Zn-Cu_3-K_6 at different values of CO space velocity.

Figure 2.6 shows the influence of the partial pressure of H_2 on the rate of CO conversion and hydrocarbon formation when CO conversion (X_{CO}) is ca. 17%. A positive influence of the hydrogen partial pressure on the hydrocarbon formation and CO conversion rate is observed. These data show that hydrocarbon synthesis reactions are first-order with respect to the H_2 partial pressure.

Table 2.5 shows the influence of the H_2 partial pressure on the reaction selectivity and products olefinicity (as the *1*-pentene/*n*-pentane ratio) at the same CO conversion level (~17%) and same CO partial pressure. Higher H_2 partial pressures lead to lighter hydrocarbons. Methane selectivity increases and C_{5+} hydrocarbons selectivity decreases with increasing H_2 pressure. As H_2 pressure increases, the relative surface coverage of H-atoms increases relative to CO and the probability of chain termination by hydrogenation increases relative to chain growth, leading to shorter reaction products. CO_2 selectivity depend on H_2 pressure, because oxygen formed via CO dissociation is rejected via reactions with chemisorbed hydrogen instead of CO. The olefin content (e.g. *1*-pentene/*n*-pentane ratio) decreases as H_2 pressure increases because of the higher probability of alkyl chain termination via hydrogenation vs.β-hydrogen abstraction.

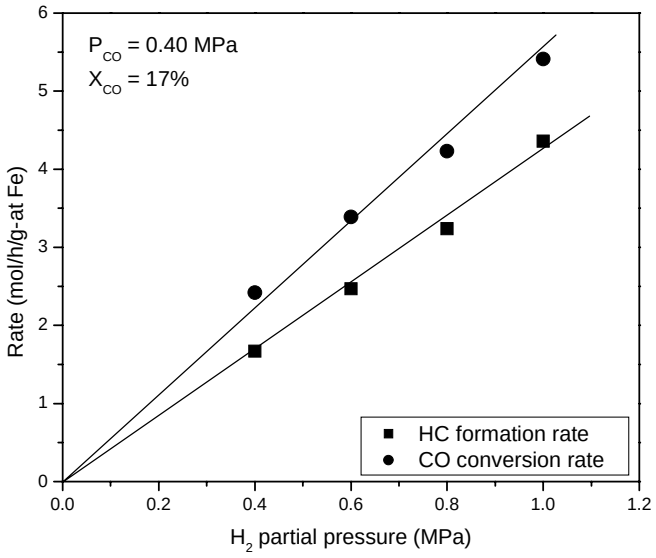

Figure 2.6. CO conversion rate and hydrocarbons formation rate over Fe-Zn-Cu_3-K_6 as a function of the H_2 partial pressure (P_{CO} = 0.40 MPa, CO conversion 17%).

Table 2.5. Influence of H_2 partial pressure on the reaction products distribution.

Pressure (MPa)		Selectivity (%, C basis)				*1*-$C_5^=$/*n*-C_5
CO	H_2	CO_2	C_1 [a]	C_2-C_4 [a]	C_{5+} [a]	
0.40	0.40	35.1	2.6	7.3	90.1	4.50
0.40	0.60	26.8	3.3	9.7	87.0	3.70
0.40	0.80	23.5	3.7	10.3	86.2	3.24
0.40	1.00	18.1	5.0	14.6	80.5	2.85

a. CO_2-free.

Reaction conditions: 508 K, CO conversion ~17%.

2.4.2. Influence of CO partial pressure on reaction rates and product selectivity.

The effects of CO partial pressure on the catalytic activity and selectivity were also examined on Fe-Zn-Cu_3-K_6 at 508 K and constant H_2 pressure (P_{H2} = 1.20 MPa) with varying CO partial pressures (P_{CO}= 0.25, 0.36, 0.54, 0.80 and 1.20 MPa). Figure 2.7 shows the influence of CO partial pressure on the CO conversion at different values of CO space velocity

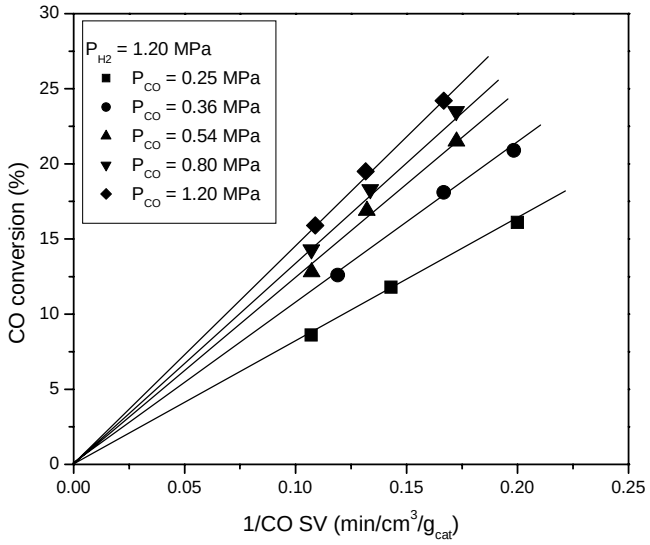

Figure 2.7. Influence of CO partial pressure on the CO conversion over Fe-Zn-Cu_3-K_6 at different values of CO space velocity.

.

CO conversion rates increased with increasing CO pressure. Figure 2.8 illustrates the influence of CO pressure on CO conversion and hydrocarbon formation for CO conversions (X_{CO}) of ~17%. At low CO pressures, CO conversion and hydrocarbon synthesis rates are positive order on CO pressure, but approach zero-order as the CO pressure increases.

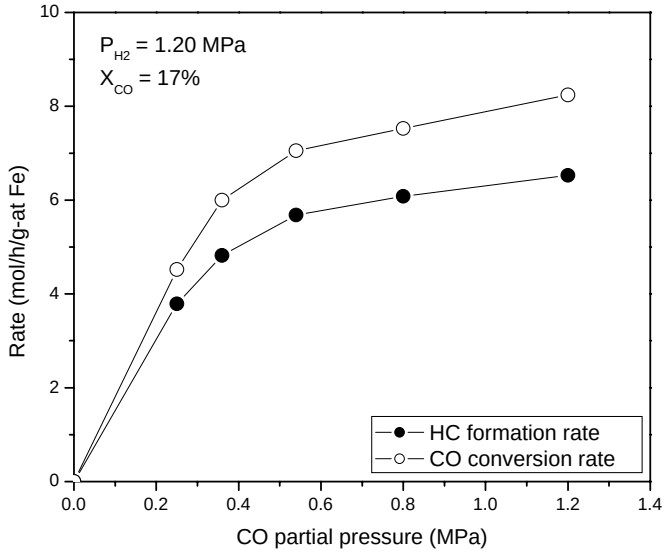

Figure 2.8. CO conversion rate and hydrocarbons formation rate over Fe-Zn-Cu_3-K_6 as a function of the CO partial pressure (P_{H2} = 1.20 MPa, CO conversion 17%).

Table 2.6 shows the influence of the CO partial pressure on the reaction selectivity and products olefinicity (as *1*-pentene/*n*-pentane ratio) at the same CO conversion level (~17%) and same H_2 partial pressure.

Table 2.6. Influence of CO partial pressure on products selectivity

Pressure (MPa)		Selectivity (%, C base)				*1*-$C_5^=$/*n*-C_5
CO	H_2	CO_2	C_1 [a]	C_2-C_4 [a]	C_{5+} [a]	
0.25	1.20	18.1	5.4	16.2	78.4	2.55
0.36	1.20	19.0	4.4	12.6	83.0	2.48
0.54	1.20	19.6	3.3	10.8	85.9	2.57
0.80	1.20	20.5	2.8	9.8	87.4	2.65
1.20	1.20	21.5	2.2	8.3	89.5	2.84

a. CO_2-free.

Reaction conditions: 508 K, CO conversion ~17%.

According to the Table 2.6, an increase of the CO partial pressure results in heavier hydrocarbons. As it was shown previously in Table 2.5, methane selectivity increases and C_{5+} hydrocarbons selectivity decreases with increasing the H_2/CO ratio of the synthesis gas. Furthermore, it is clear that the dependence of the carbon dioxide selectivity with the CO partial pressure is not as strong as the dependence with the H_2 partial pressure (shown in Table 2.5). As a consequence of the higher CO partial pressure in the synthesis gas, the rate of CO_2 formation *via* the reaction of chemisorbed carbon monoxide (CO*) and chemisorbed oxygen (O*) can be enhanced, which is known as a primary CO_2 selectivity. In addition, this increase of the CO partial pressure can also lead to higher forward water-gas shift reaction rates (secondary CO_2 selectivity). It can be also observed in Table 2.6 that the *1*-pentene/*n*-pentane is almost independent of the CO partial pressure. The *1*-oleffin/*n*-paraffin ratio is determined by the relative reaction rates of chain termination by hydrogenation and by β-abstraction. Our results show that the relative rate of these reactions is not affected by the CO partial pressure in the synthesis gas.

2.4.3. Mechanism and kinetics of hydrocarbons formation.

The mechanism of the hydrocarbons formation is still not fully understood. Among the several mechanisms proposed in the literature for the Fischer-Tropsch Synthesis, the most plausible one seems to be the surface carbide mechanism by CH_2 insertion (G.P. van der Laan and A.A.C.M. Beenackers, Catal. Rev. Sci. Eng. 41 (1999) 255). However, it is not clear how the monomer formation takes place. The CH_2 units can be formed *via* hydrogenation of dissociated or undissociated CO. On the other hand, hydrogen can react via either the dissociative adsorbed state or in the molecular state, although this latter mechanism seems to be highly improbable. In this work, we have proposed several mechanisms (Table 2.7) for hydrocarbons formation over iron-based catalysts by assuming different sets of equilibrium steps.

Table 2.7. Set of elementary reactions for the Fischer-Tropsch Synthesis.

Model	Elementary reactions		Model	Elementary reactions
FT-1	1. CO + * ⇆ CO* 2. H_2 + 2 * ⇆ 2 H* 3. CO* + * → C* + O* 4. C* + H* → CH* + * 5. CH* + H* → CH_2* + * 6. O* + H* → OH* + * 7. OH* + H* → H_2O* 8. H_2O* ⇆ H_2O + *		**FT-2**	1. CO + * ⇆ CO* 2. H_2 + 2 * ⇆ 2 H* 3. CO* + * ⇆ C* + O* 4. C* + H* → CH* + * 5. CH* + H* → CH_2* + * 6. O* + H* → OH* + * 7. OH* + H* → H_2O* 8. H_2O* ⇆ H_2O + *
FT-3	1. CO + * ⇆ CO* 2. H_2 + 2 * ⇆ 2 H* 3. CO* + * ⇆ C* + O* 4. C* + H* ⇆ CH* + * 5. CH* + H* → CH_2* + * 6. O* + H* → OH* + * 7. OH* + H* → H_2O* 8. H_2O* ⇆ H_2O + *		**FT-4**	1. CO + * ⇆ CO* 2. CO* + * ⇆ C* + O* 3. C* + H_2 → CH_2* 4. O* + H_2 → H_2O* 5. H_2O* ⇆ H_2O + *
FT-5	1. CO + * ⇆ CO* 2. H_2 + 2 * ⇆ 2 H* 3. CO* + H* → COH* + * 4. COH* + H* → COH_2* + * 5. COH_2* + * → CH_2* + O* 6. O* + H* → OH* + * 7. OH* + H* → H_2O* 8. H_2O* ⇆ H_2O + *		**FT-6**	1. CO + * ⇆ CO* 2. H_2 + 2 * ⇆ 2 H* 3. CO* + H* ⇆ COH* + * 4. COH* + H* → COH_2* + * 5. COH_2* + * → CH_2* + O* 6. O* + H* → OH* + * 7. OH* + H* → H_2O* 8. H_2O* ⇆ H_2O + *
FT-7	1. CO + * ⇆ CO* 2. H_2 + 2 * ⇆ 2 H* 3. CO* + H* ⇆ COH* + * 4. COH* + H* ⇆COH_2* + * 5. COH_2* + * → CH_2* + O* 6. O* + H* → OH* + * 7. OH* + H* → H_2O* 8. H_2O* ⇆ H_2O + *		**FT-8**	1. CO + * ⇆ CO* 2. CO* + H_2 → COH_2* 3. COH_2* + * → CH_2* + O* 4. O* + H_2 → H_2O* 5. H_2O* ⇆ H_2O + *
FT-9	1. CO + * ⇆ CO* 2. CO* + H_2 ⇆ COH_2* 3. COH_2* + * → CH_2* + O* 4. O* + H_2 → H_2O* 5. H_2O* ⇆ H_2O + *			

Table 2.8 summarizes the final form of the different rate expressions (Langmuir-Hinshelwood) for the 9 possible kinetics models considered. It can be seen that the pressure dependency of CO and H_2 in the numerator ranges from ½ to 1, and from 0 to 1, respectively. The denominator consists of the individual contributions of significantly abundant species on the catalyst surface. Although the catalyst surface is composed by different adsorbed species, such as carbon, carbon monoxide, hydrogen, alkyl chains, etc, we have assumed that the most abundant species on the surface are free active sites (*) and undissociated CO (CO*) or carbidic species (C*), depending on the kinetic model. No water inhibition term (H_2O*) has been considered in this work.

Table 2.8. Reaction rate expressions derived from the different Fischer-Tropsch Synthesis mechanisms.

Model	Kinetic equation	k	a
FT-1	$r = \frac{k\,P_{CO}}{\left(1 + a\frac{P_{CO}}{P_{H_2}^{1/2}}\right)^2}$	K_1k_3	$\frac{K_1k_3}{K_2^{1/2}k_4}$
FT-2	$r = \frac{k\,P_{CO}^{1/2}P_{H_2}^{1/2}}{\left(1 + aP_{CO}^{1/2}\right)^2}$	$(K_1K_2K_3k_4k_6)^{1/2}$	$(K_1K_3k_6/k_4)^{1/2}$
FT-3	$r = \frac{k\,P_{CO}^{1/2}P_{H_2}^{3/4}}{\left(1 + a\frac{P_{CO}^{1/2}}{P_{H_2}^{1/4}}\right)^2}$	$(K_1K_2^{1/2}K_3K_4k_5k_6)^{1/2}$	$\left(\frac{K_1K_3k_6}{K_2^{1/2}K_4k_5}\right)^{1/2}$
FT-4	$r = \frac{k\,P_{CO}^{1/2}P_{H_2}}{1 + aP_{CO}^{1/2}}$	$(K_1K_2k_3k_4)^{1/2}$	$(K_1K_2k_4/k_3)^{1/2}$
FT-5	$r = \frac{kP_{CO}P_{H_2}^{1/2}}{(1 + aP_{CO})^2}$	$K_1K_2^{1/2}k_3$	K_1
FT-6	$r = \frac{kP_{CO}P_{H_2}}{(1 + aP_{CO})^2}$	$K_1K_2K_3k_4$	K_1
FT-7	$r = \frac{kP_{CO}P_{H_2}}{(1 + aP_{CO})^2}$	$K_1K_2K_3K_4k_5$	K_1
FT-8	$r = \frac{kP_{CO}P_{H_2}}{1 + aP_{CO}}$	K_1k_2	K_1
FT-9	$r = \frac{kP_{CO}P_{H_2}}{(1 + aP_{CO})^2}$	$K_1K_2k_3$	K_1

According to mechanistic considerations based on the literature, along with the results of H_2 and CO partial pressure dependence shown in Figures 2.6 and 2.8 respectively, mechanisms FT-3 and FT-6 seem to be the most appropriate in describing the hydrocarbon formation pathway over Fe-based catalysts. It should be noted that models FT-6 and FT-7 are kinetically indistinguishable, and consequently, the same kinetic conclusions can be applied for both models simultaneously.

The observed rate of hydrocarbon formation has been fitted to the linearized kinetic expressions derived from mechanisms FT-3 and FT-6:

According to the model FT-3: $r = \dfrac{k\,P_{CO}^{1/2}P_{H_2}^{3/4}}{\left(1+a\dfrac{P_{CO}^{1/2}}{P_{H_2}^{1/4}}\right)^2}$

or in linearized form: $\left(\dfrac{P_{CO}^{1/2}\cdot P_{H_2}^{3/4}}{r}\right)^{1/2} = \dfrac{1}{k^{1/2}} + \dfrac{a}{k^{1/2}}\dfrac{P_{CO}^{1/2}}{P_{H_2}^{1/4}}$

In the same way, the model FT-6 yields to the following expression:

$$\left(\frac{P_{CO}\cdot P_{H_2}}{r}\right)^{1/2} = \frac{1}{k^{1/2}} + \frac{a}{k^{1/2}}P_{CO}$$

Figures 2.9 and 2.10 display the linearized plots for the model FT-3 and FT-6 here proposed.

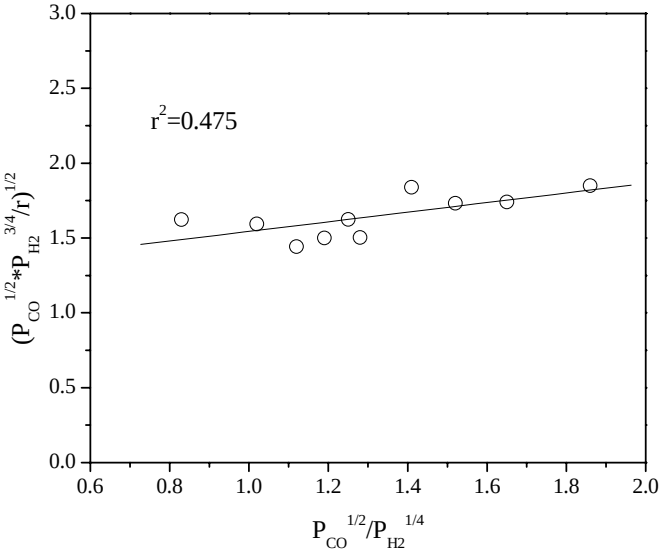

Figure 2.9. Fitting of the linearized rate expression derived from model FT-3 with the observed rate of hydrocarbons formation.

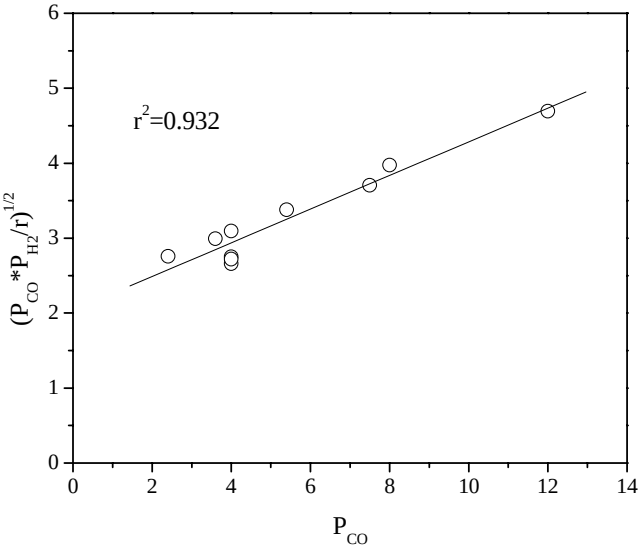

Figure 2.10. Fitting of the linearized rate expression derived from model FT-6 with the observed rate of hydrocarbons formation.

The observed rate of hydrocarbon formation is poorly represented by the rate expression obtained with the elementary reactions proposed in model FT-3 (Figure 2.9), in which the monomer formation takes place by hydrogenation of dissociated CO. However, the experimental data are much better described by the model FT-6, where the monomer is formed by hydrogenation of associatively adsorbed carbon monoxide. Therefore, and according to our results, it seems that hydrocarbons are formed over Fe-based catalysts following the mechanism named as FT-6 or FT-7, where the formation of the surface monomer is controlled by the hydrogenation of associatively adsorbed CO.

Nevertheless, the mechanism proposed should be improved in order to obtain a better fitting of the experimental data. This work will be done during the following reporting period.